Appl. Phys. B 76, 441–449 (2003)
DOI: 10.1007/s00340-003-1140-8

**Applied Physics B**
**Lasers and Optics**

J. HENNINGSEN✉
J. HALD

# Quantitative analysis of dilute mixtures of $SO_2$ in $N_2$ at 7.4 μm by difference frequency spectroscopy

Danish Institute of Fundamental Metrology, Matematiktorvet 307, 2800 Lyngby, Denmark

**Received: 16 January 2003/Revised version: 19 February 2003**
**Published online: 9 April 2003 •** 

**ABSTRACT** We describe a 7.4-μm source based on difference frequency generation with 6.5 mW of 1278-nm radiation from an extended cavity laser and 66 mW of 1544-nm radiation from another extended cavity laser, amplified in an erbium-doped fibre amplifier. Optimum focusing of the input beams in the $5 \times 5 \times 10$-$mm^3$ $AgGaSe_2$ crystal, and the spatial and temporal characteristics of the output beam, are determined. The source is used for accurate determination of line parameters for selected lines of the $\nu_3$ band of $SO_2$, centred at 1361 $cm^{-1}$. Subsequently, these lines are used for performing quantitative analysis of gas mixtures containing $SO_2$ at concentration levels down to 4 ppm without relying on any calibration with certified gas mixtures. This demonstrates the potential of infrared spectroscopy as a primary method for low-concentration gas analysis.

**PACS** 07.88.+y; 33.20.Ea; 42.62.Eh; 42.62.Fi; 42.65.Ky; 42.68.Ca

## 1 Introduction

The detection of trace amounts of specific molecules in a more or less well-characterised gaseous matrix is a basic problem in environmental science, as well as in many aspects of process control. The use of the highly specific infrared absorption spectra of molecules in many ways represents an ideal solution, and techniques based on absorption of incoherent radiation have established themselves firmly, be it as Fourier-transform spectroscopy, or as selective absorption of radiation from filtered white-light sources. In these cases quantitative information is derived by comparing the absorption in the unknown gas mixture with absorption in a certified mixture usually produced by gravimetric methods. However, if resolved lines can be observed with a narrowband source which does not corrupt the line profile, a measurement of the absorbance over a known path length can be directly translated into information about the number density of the absorbing molecule without relying on comparison with a reference standard. In such cases infrared spectroscopy may then be considered as a primary method for concentration measurements [1].

✉ Fax: +45-4593/1137, E-mail: jh@dfm.dtu.dk

The use of laser spectroscopy in the mid infrared, where molecules have their fundamental vibrational absorption bands, is hampered by the lack of convenient monochromatic sources. Diode lasers based on small-gap semiconductors have been available for almost 30 years and have been extensively used for spectroscopy in research environments, as reviewed in [2]. However, it has been difficult for these lasers to penetrate into the realm of industrial applications, mainly due to the need for cryogenic cooling. A more recently developed alternative is the quantum cascade laser [3], where the naturally occurring small band gaps of materials such as lead–tin telluride are replaced by custom-designed electronic energy levels in carefully tailored microstructures based on gallium arsenide. These lasers have now been developed to the point where pulsed emission can be obtained at room temperature [4]. However, their long-term performance remains to be investigated.

The concept of using visible and near-infrared lasers for difference frequency generation (DFG) in optically non-linear crystals dates back to 1971 [5], and since then a wide range of materials and laser combinations have been used. The use of diode lasers in conjunction with $AgGaSe_2$ for the wavelength range 7–9 μm was suggested by Simon et al. [6], and two systems have been described in the literature. Petrov et al. [7] describe an 8.7-μm source based on a 1554-nm DFB laser amplified by an Er:Yb fiber amplifier, and a 1319-nm Nd:YAG laser, and with 370-mW and 29-mW power incident on the 10-mm crystal they report a generated power of about 100 nW. Sumpf et al. [8] use a 6-mW extended cavity laser covering the 1504–1589-nm range and an 8-mW single-mode Fabry–Pérot laser at 1290 nm, and report an output power of about 10 nW from a 40-mm crystal. For both of these systems the performance was demonstrated by measurements on $SO_2$, but no attempts were made to exploit the potential for precision measurements.

The present work aims at demonstrating the feasibility of using DFG sources as a basis for quantitative low-concentration trace-gas analysis without the need for calibration against a known standard. Section 2 contains a description of the experimental setup and a characterisation of the DFG source. Section 3 describes measurements performed on pure $SO_2$ in order to determine the line parameters needed for subsequent quantitative analysis, and in Sect. 4 these parameters are used to analyse a range of gas mixtures derived from

a 540-ppm certified mixture of $SO_2$ in $N_2$. Uncertainty estimates are given in Sect. 5, and Sect. 6 contains a discussion and the conclusions.

## 2 The experimental setup

### 2.1 *The DFG source*

A main rationale behind the experimental setup shown in Fig. 1 is that it must be built from elements which are commercially available, and with proven reliability. One input source is a New Focus Vortex laser, which is an extended cavity laser with fixed grating, providing 7 mW of output power at 1278.309 nm. The second input source is a New Focus extended cavity laser, model 6262, tunable from 1510 to 1580 nm, whose 3-mW output is amplified to 70 mW in an erbium-doped fibre amplifier manufactured by BTI Photonics. The polarization of each beam is controlled with a $\lambda/2$ plate, and they are combined in a polarization beam splitter. The combined beams are focused with a common, broad-band AR-coated 150-mm-focal length lens onto a $5 \times 5 \times 10\,\mathrm{mm}^3$ crystal of $AgGaSe_2$, mounted on a translation–rotation stage. The crystal is produced by EKSMA, Lithuania, and is cut for 90° non-critical phase matching. The transmitted signals are focused on a $1 \times 1\text{-mm}^2$ Hamamatsu P3257-10 liquid nitrogen cooled MCT detector, with an off-axis parabolic mirror of 5-cm focal length, and the near-infrared radiation is blocked by an interference filter.

### 2.2 *Optimum focusing*

The dependence on focusing was studied by varying the focal length of the common lens, as well as by introducing additional lenses in the 1278-nm beam before it reaches the beam splitter. The results of varying the common lens are shown in Fig. 2, and an optimum is found for a focal length of about 150 mm. No significant improvement was observed when introducing additional lenses in the 1278-nm beam to compensate for the chromaticity.

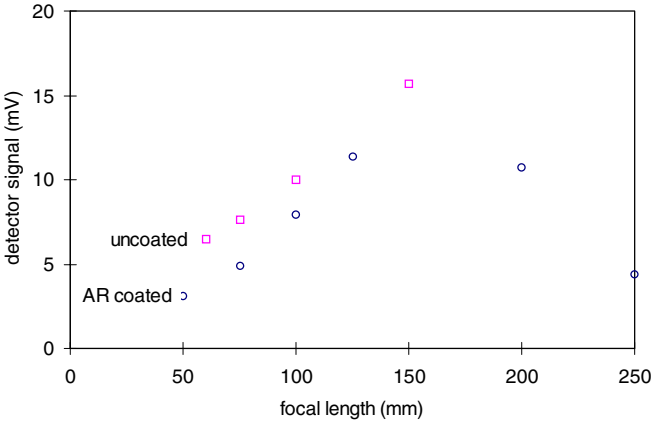


**FIGURE 2** Difference frequency signal as a function of the focal length of the focusing lens

| λ (nm) | θ (mrad) | $w_0$ (μm) | $z_R$ (mm) |
|---|---|---|---|
| 1278 | 4.9 | 83 | 17.1 |
| 1544 | 9.0 | 54 | 6.0 |
| 7418 | 26.6 | 89 | 3.3 |

**TABLE 1** Far-field divergence ($\theta$), beam-waist radius ($w_0$), and Rayleigh length ($z_R$) for the three beams

The fundamental Gaussian character of all three beams was verified by analysing the beam cross section with a knife edge, and the beam characteristics were determined with results as given in Table 1. The radii of the beam waists, which are located within the crystal, are determined from the far-field divergence. We find that the beam waists are significantly larger than those used in both [7] and [8].

### 2.3 *Phase matching*

Phase matching was studied as a function of the rotation angle of the crystal over the range ±10°. The 1278-nm

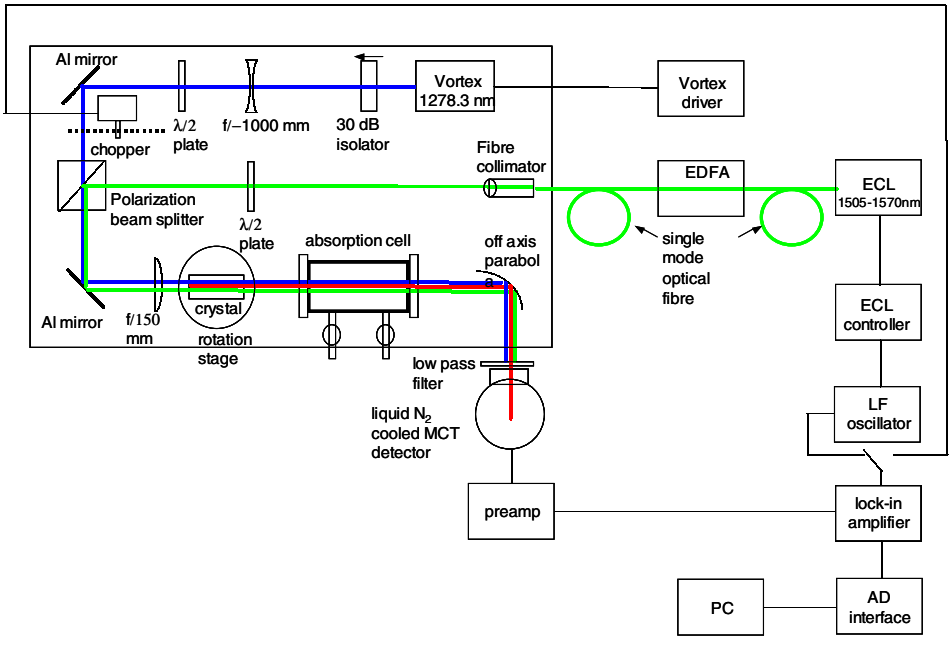


**FIGURE 1** Experimental layout of difference frequency source

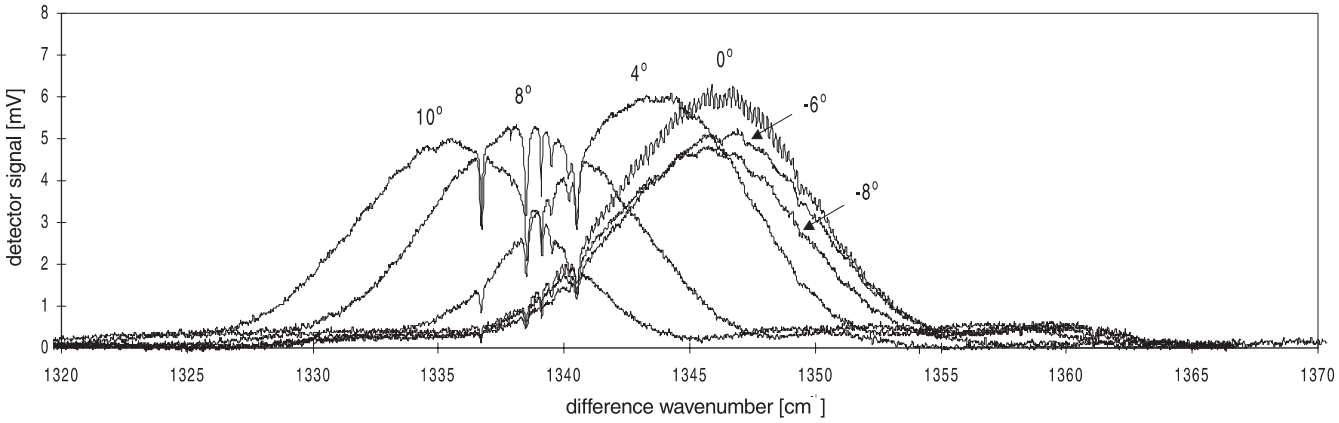


**FIGURE 3** Difference frequency output as a function of difference wavenumber for different angles of incidence on the non-linear crystal

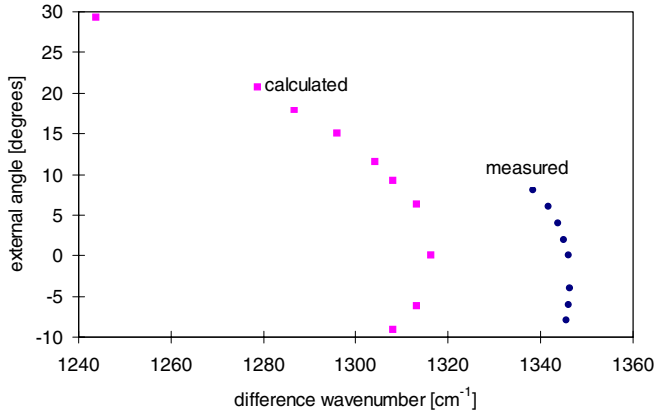


**FIGURE 4** Relation between external angle of incident beams and the phase-matching wavenumber

wavelength remained fixed while the 1544-nm wavelength was scanned with results as shown in Fig. 3. At an angle of 0°, corresponding to perpendicular incidence on the end face of the crystal, Fabry–Pérot oscillations are seen with a free spectral range of 5.5 GHz, arising from reflections at the imperfectly AR-coated surfaces. A weaker oscillation with a period of 33 GHz is caused by internal reflections in the 1-mm-thick Ge substrate of the interference filter. The absorption lines centrally located on the 8° curve originate from water vapour in the 56-cm path from the crystal to the detector. In Fig. 4 the difference wavenumber for optimum phase matching is plotted as a function of the rotation angle, and a comparison with calculations based on the Sellmeyer coefficients given in [9] confirms the discrepancy noted in [8], with optimum phase matching occurring at a wavenumber about 20 $cm^{-1}$ lower than predicted.

### 2.4 *Conversion efficiency*

According to the manufacturer's specifications, the MCT detector has a responsivity at 7.4 μm of 2557 V/W. The maximum measured detector voltage was 36 mV, and taking into account the 2000 times amplification of the preamplifier and the 75% transmission of the interference filter, this means that a power of about 9.4 nW leaves the crystal. The beam waist of the focused radiation falling on the detector is significantly smaller than its 1 × 1-$mm^2$ area, so no radiation misses the detector. The near-infrared power reaching the crystal is about 6.5 mW at 1278 nm, and 66 mW at 1544 nm, leading to a conversion efficiency of

$$\eta = \frac{9.4 \times 10^{-9}}{6.5 \times 10^{-3} \times 66 \times 10^{-3}} = 2.2 \times 10^{-5}\,\mathrm{W}^{-1}. \quad (1)$$

### 2.5 *Signal-to-noise ratio*

Based on the manufacturer's specifications the detector has a noise equivalent power of $\mathrm{NEP} = 2.7 \times 10^{-12}\,\mathrm{W}/\sqrt{\mathrm{Hz}}$ at the applied bias current of 15 mA. The total noise was measured at various power levels, and it was found that the signal/noise ratio S/N can be expressed as

$$\mathrm{S/N} = \frac{P}{\sqrt{(2.2 \times 10^{-3} P)^2 + B \times \mathrm{NEP}^2}}, \quad (2)$$

where $B$ is the noise bandwidth in Hz. Note that while the detector contribution can be reduced by decreasing the noise bandwidth, this is not the case for the source term. The reason for this is that the relative source noise of $2.2 \times 10^{-3}$ originates from etalon effects in the optical components, and while an increase of the time constant in the detection system will reduce the noise on a time scale shorter than the time constant, the noise will be found to persist if the signal is measured over longer times, due to drift of the fringes. According to (2) the S/N ratio will tend towards a limiting value of 450 for large DFG power, and at our maximum power we have S/N = 440, i.e. close to the optimum value.

### 2.6 *Stability*

The long- and short-term stability can be assessed from measurements reported in Sect. 3. Both laser sources were free running and the setup was located in a laboratory with temperature variations over a day of up to 2 °C. During the 3.5-h time span used for recording the spectra shown in Fig. 5, the average drift was 1.3 MHz/min with a maximum drift of 2.8 MHz/min. The short-term stability can be assessed from analysis of the spectral line profiles. When plotting the Lorentz contribution to the line width as a function

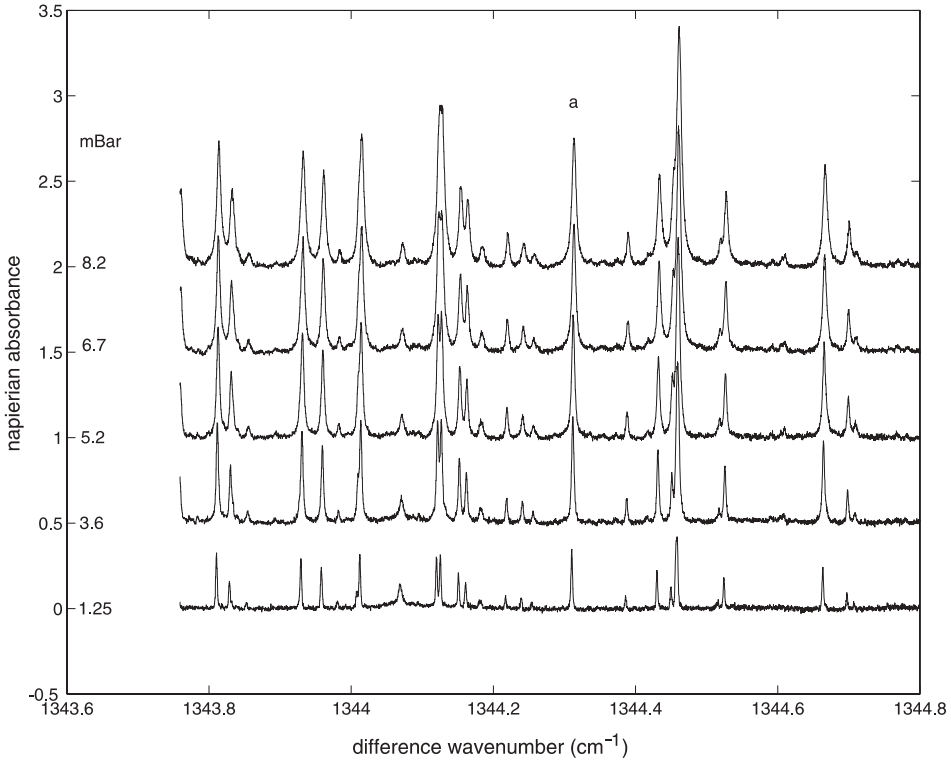


**FIGURE 5** Absorbance spectra for $SO_2$ recorded for 11.4-mm cell at five different pressures

of pressure, a straight line is expected with a zero intercept determined by the spectral width of the source. From analysis of 18 lines we find a mean value of the zero intercept of $1.3 \pm 0.8$ MHz, which may thus be taken as an estimate of the spectral width of the difference frequency source.

### 2.7 *Cells*

The DFG source is used in conjunction with two cells. Cell I with a length of 11.4 mm is used in a sealed configuration for performing measurements on pure $SO_2$ with the purpose of determining line parameters for the relevant lines. In order to achieve a more favourable ratio between volume and surface, this cell is connected to a reservoir of about 1000 cm$^3$. Cell II is a White cell with 20-cm base length, and 12 passes provide a total path length of 245 cm. This cell is used in a flow configuration for performing measurements on trace quantities of $SO_2$ in different backgrounds. Both cells are provided with windows of $CaF_2$.

## 3 Determination of line parameters

The experimentally measured quantity is the absorbance $\alpha L$, which through Beer's law

$$I(L) = I(0)\exp(-\alpha L) \tag{3}$$

governs the attenuation of a monochromatic signal as it propagates the distance $L$ in the gas. The Napierian absorbance is determined as $\alpha L = \ln(I_{p=0}/I_p)$ from the transmitted signal $I_{p=0}$ at zero pressure and $I_p$ at the actual pressure. Frequency scans are performed by leaving the 1278-nm source free running, and scanning the 1544-nm source. Long scans with moderate resolution are performed by rotating the grating of the extended cavity, while the highest resolution is obtained by scanning over a range of about 33 GHz with the piezo controlling the length of the extended cavity. Part of the 1544-nm signal is sent through a Fabry–Pérot interferometer with 2.026-GHz free spectral range, and the transmitted signal provides sharp equidistant markers which are subsequently used for transforming the independent variable of the spectra from piezo voltage to frequency. Apart from the source, the setup is similar to that described previously [10].

In order to quantify the results of measurements at low concentrations, it is imperative that line strengths and broadening parameters are accurately known for the selected lines. We have chosen the range 1343.8 cm$^{-1}$ to 1344.9 cm$^{-1}$, which in addition to strong $SO_2$ lines also contains a line of $H_2O$ with a strength that makes it convenient for monitoring water at concentrations typical of ambient air. Measurements on pure $SO_2$ were performed on cell I, filled with 99.99% $SO_2$ from Aldrich at pressures ranging from 0 mbar to 10.2 mbar as measured with a MKS Baratron pressure gauge. At each pressure the signal transmitted through the cell was recorded in 5000 steps, corresponding to a resolution of 6.6 MHz. The integration time of the lock-in amplifier was 0.1 s, and a delay of 0.24 s per step ensured that even the narrowest lines could be recorded without risk of distortion.

Absorbance spectra for five pressures are shown in Fig. 5, where the absolute wavenumbers are based on using the HITRAN value of 1344.31026 cm$^{-1}$ for line *a* as reference [11]. Individual lines were fitted to Voigt functions with calculated Doppler broadening, using as the four free parameters the coefficient multiplying the line-shape function, the Lorentz-broadening coefficient, the line-centre frequency, and a constant background term. For overlapping lines we used an it-

erative approach where results for one iteration were used for eliminating the effect of neighbouring lines in the next iteration. The upper trace in Fig. 6 shows a section of the recorded spectrum at 8.2 mbar together with fits of eight lines labelled *a*–*h*, while the lower trace shows the residual. The results of the analysis are summarised in Table 2, where the line-centre wavenumbers are those given in [11]. Lines *e*, *f* form a doublet which cannot be resolved even at the lowest pressure, and it has been analysed as two identical lines with the separation 54 MHz given in HITRAN.

The absorption coefficient at frequency $\nu$ is given by

$$\alpha(\nu - \nu_0) = SNg(\nu - \nu_0)\,, \tag{4}$$

where $S$ is the line strength, $g(\nu - \nu_0)$ is the area-normalised line-shape function centred at frequency $\nu_0$, and $N$ is the number density, which can be expressed in terms of the pressure $p$, the absolute temperature $T$, and the Boltzmann constant $k$ as

$$N = \frac{p}{kT}\,. \tag{5}$$

By integrating (4) over all frequencies it is seen that $S$ measures the integrated absorption independently of the functional form of $g(\nu - \nu_0)$. $S$ is determined by the transition dipole moment and by the number of molecules present in the lower and upper states connected by the transition. While the dipole moment reflects the charge distribution in the molecule, and can therefore be considered as a constant of nature, the level populations depend on temperature through a Boltzmann factor and through the temperature dependence of the partition function. In principle, different temperatures could be associated with the different degrees of freedom of the molecule, but under our conditions we may assume equilibrium, so that the rotational and vibrational temperatures may be taken equal to the translational temperature $T$. It has become customary to use the temperature 298 K as a reference temperature for line strengths, and all values quoted in [11] refer to this temperature. All measurements reported in this paper are performed in a ±2-K interval around 298 K, and deviations from the reference temperature will be accounted for as an uncertainty contribution.

According to (3)–(5) the coefficient multiplying $g(\nu - \nu_0)$ in the four-parameter Voigt fit equals $LSp/kT$, and the line strength is derived from the slope of a linear least-square fit of this coefficient plotted as a function of pressure. The results are given in Table 2. For comparison the HITRAN values are listed in column 4, and our results confirm the observation of [8] that they are generally too large.

The Lorentz self-broadening parameters (HWHM) derived from the Voigt fits are given in column 6. HITRAN lists a common value of $0.4\,\mathrm{cm^{-1}/atm}$, corresponding to 11.8 MHz/mbar for all lines. This corresponds reasonably well to our result for the strong lines, whereas we find significantly smaller broadening coefficients for the weaker lines.

Nitrogen broadening parameters were determined from measurements in the White cell over the pressure range up to 100 mbar with results as given in the last column of Table 2. Since the pressures are higher than those used for determination of self-broadening, the rather strong overlap of the lines leads to a larger uncertainty of about 10% for the strongest lines, and it was not possible to derive broadening parameters for the weak lines *b* and *g*. Nevertheless, it is clearly seen that the line to line variations tend to be smaller than for self-broadening.

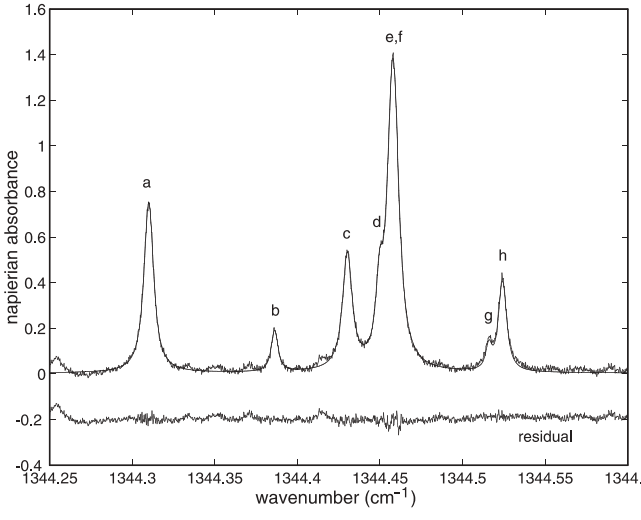


**FIGURE 6** Absorbance spectrum at 8.2 mbar together with Voigt fit of eight lines (*upper trace*) and residual (*lower trace*)

## 4 Analysis of dilute mixtures

Low concentrations of $SO_2$ in $N_2$ were generated as shown in Fig. 7. By dynamic mixing of pure nitrogen through a 0–100-mL/min flow controller with a certified mixture of 540-ppm $SO_2$ in nitrogen through a 0–10-mL/min controller, concentrations were generated down to about 50 ppm. The gas is sampled at ambient pressure, and the pressure in the cell and the flow through the cell can be adjusted with the needle valves without any risk of changing the concentration.

| Line | Wavenumber ($\mathrm{cm^{-1}}$) | $S$ ($10^{-20}$ cm/mol) | $S_H$ ($10^{-20}$ cm/mol) | Ratio ($S/S_H$) | Self-broadening (MHz/mbar) | $N_2$ broadening (MHz/mbar) |
|---|---|---|---|---|---|---|
| *a* | 1344.31026 | 3.56 ± 0.13 | 4.291 | 0.83 | 11.34 ± 0.35 | 3.03 ± 0.28 |
| *b* | 1344.38567 | 0.59 ± 0.08 | 0.597 | 0.98 | 7.98 ± 0.53 | |
| *c* | 1344.42965 | 2.43 ± 0.14 | 2.942 | 0.83 | 12.33 ± 0.66 | 3.14 ± 0.29 |
| *d* | 1344.44913 | 0.82 ± 0.12 | 1.457 | 0.56 | 7.21 ± 0.91 | 2.37 ± 0.17 |
| *e* | 1344.45612 | 3.83 ± 0.12 | 4.304 | 0.89 | 13.1 ± 0.35 | 2.49 ± 0.31 |
| *f* | 1344.45793 | 3.83 ± 0.12 | 4.437 | 0.86 | 13.1 ± 0.35 | 2.49 ± 0.31 |
| *g* | 1344.51539 | 0.28 ± 0.09 | 0.378 | 0.74 | 6.15 ± 3.12 | |
| *h* | 1344.52377 | 1.56 ± 0.08 | 2.186 | 0.71 | 9.40 ± 0.29 | 2.64 ± 0.22 |

**TABLE 2** Line parameters for $SO_2$ lines used for low-concentration measurements. $S_H$ are line strengths according to HITRAN

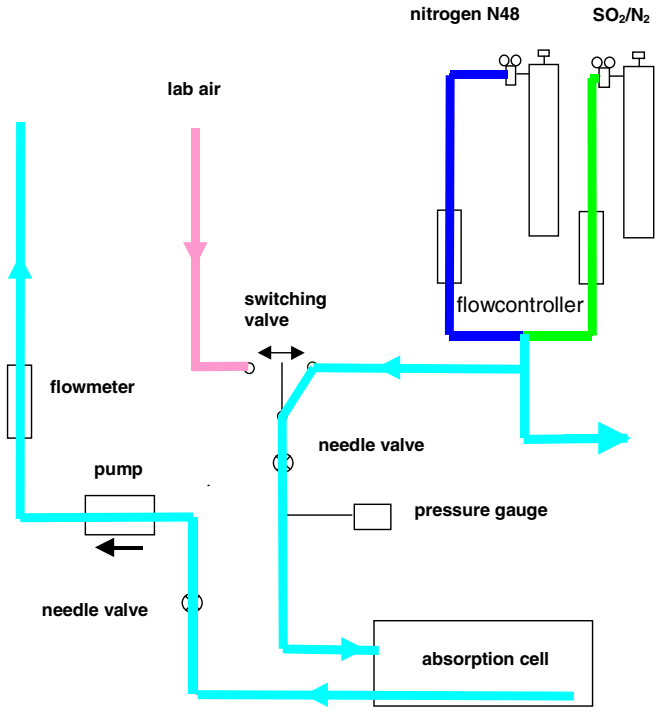


**FIGURE 7** Setup for generating low concentrations of $SO_2$ in $N_2$

Figure 8 shows absorbance spectra for five concentrations between 540 ppm and 48 ppm, all recorded at 103 mbar at a flow of about 50 mL/min at ambient pressure. For reference, the lowest pressure spectrum of pure $SO_2$ from Fig. 5 is included. The contribution to the total absorbance of a line centred at frequency $\nu_0$ to the absorbance is given by

$$L\alpha(\nu-\nu_0) = LSc\frac{p}{kT}g(\nu-\nu_0)\,, \tag{6}$$

where $L = 245\,\text{cm}$ is the absorption path length in the White cell, $S$ is the line strength as given in Table 2, $c = p(SO_2)/p_{\text{total}}$ is the concentration, $p = 103\,\text{mbar}$ is the total pressure, $k$ is the Boltzmann constant, and $T = 298\,\text{K}$ is the absolute temperature. As in (4), $g(\nu-\nu_0)$ is the area-normalised line-shape function, but this time evaluated with the coefficient for nitrogen broadening rather than for self-broadening.

In order to derive the concentrations from the spectra we focus on the line at $1344.310\,\text{cm}^{-1}$, labelled *a* in Fig. 6. It is relatively well isolated from its neighbours, and we restrict the fit to a range of $\pm 0.9\,\text{GHz}$ about the line centre in order to avoid interference. The concentrations emerge from four-parameter fits where we vary $c$, $\nu_0$, a constant background, and the nitrogen broadening parameter. For the latter we could have used the value given in Table 2, but owing to the relatively large uncertainty we have chosen to include it among the fit parameters. In Fig. 9 the five measured concentrations are plotted as a function of the concentrations evaluated from the dilution system, and a linear fit produces a slope of $1.045 \pm 0.010$ and a zero intercept of $-2\,\text{ppm}$. The measured value for the undiluted certified mixture is $560 \pm 30\,\text{ppm}$, which overlaps the $540 \pm 11\,\text{ppm}$ value stated in the certificate. The fitted value for the nitrogen broadening coefficient is $3.24 \pm 0.03\,\text{MHz/mbar}$, which is consistent with the value $3.03 \pm 0.30\,\text{MHz/mbar}$ given in Table 2.

It is of some interest to include the nearly degenerate *e*–*f* doublet in the analysis, since this will lead to a lower detection limit. For this purpose we constructed an eight-line model

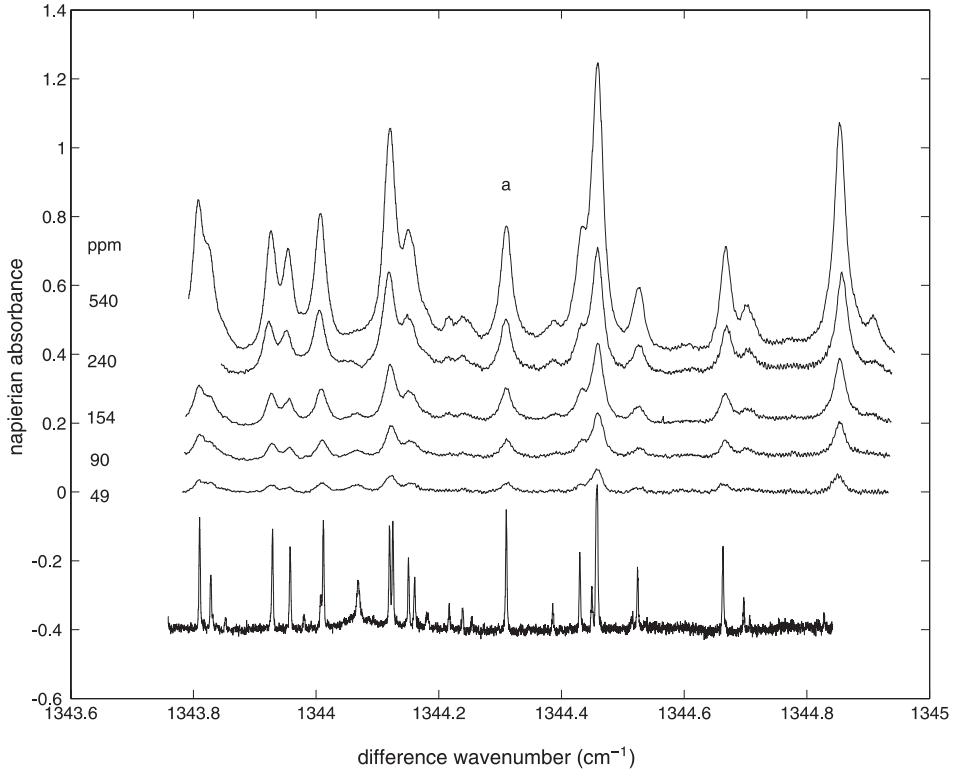


**FIGURE 8** Absorbance measurements at 98 mbar for different concentrations. *Lower trace* is low-pressure reference spectrum of pure $SO_2$

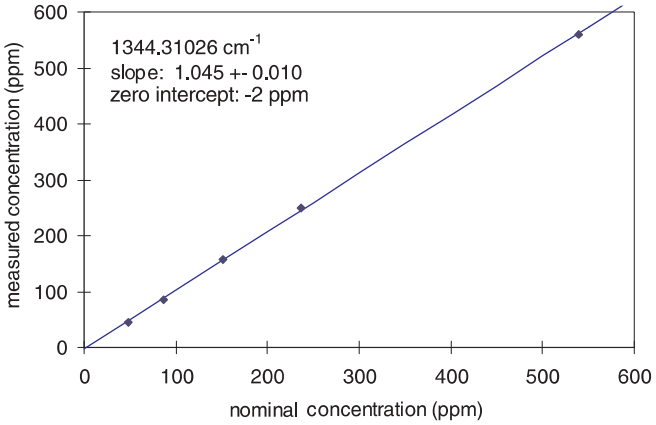


**FIGURE 9** Concentrations derived from absorbances of Fig. 8 versus nominal concentrations

function for the entire cluster of lines *a–h*, using the wave numbers and line strengths of Table 2. Again we chose to fit the broadening parameter, assuming a common value for all lines. Using this procedure, a plot similar to Fig. 9 produces a slope of $0.974 \pm 0.019$ and a zero intercept of $-9$ ppm. The value found for the undiluted certified mixture is 524 ppm, which is again consistent with the certificate value. We shall not attempt to evaluate the uncertainty in this case, since it is difficult to estimate the effect of the assumption of a common line width.

The individual concentrations are given in Table 3. The lower graph of Fig. 10 compares the experimental recording

| Nominal conc. (ppm) | One-line fit (ppm) | Eight-line fit (ppm) |
|---|---|---|
| 48.0 | $46 \pm 6$ | 36 |
| 87.7 | $86 \pm 7$ | 77 |
| 150.7 | $158 \pm 10$ | 140 |
| 236.5 | $250 \pm 14$ | 215 |
| 540 | $560 \pm 30$ | 524 |

**TABLE 3** Measured concentrations for one-line fit of line *a* and for eight-line fit of lines *a–h*

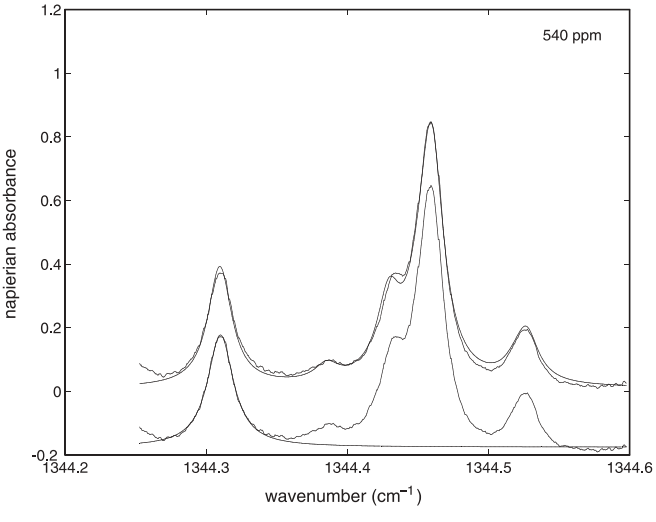


**FIGURE 10** Two-parameter fit of absorbance for undiluted certified gas mixture to eight-line model function, assuming common collision broadening (*upper graph*), and fit to line *a* alone (*lower graph*)

with the Voigt profile for line *a* evaluated with the parameters of Table 2. The upper graph shows a fit of eight lines with line centres and line strengths as given in Table 2, but assuming a common, fitted Lorentzian broadening. The degradation of the fit around line *a* shows that the assumption of a common line width is not optimum. However, using the individual values given in Table 2 for all eight lines makes the fit even worse, and we must conclude that the individual broadening parameters have not be determined with sufficient accuracy.

### 4.1 *Wavelength modulation*

For generating concentrations down to 4 ppm, the $N_2$ flow controller in Fig. 7 was changed to 0–1000 mL/min. Since a small absorbance shows up as a small difference between two large signals, it is here advantageous to use wavelength-modulation techniques. The 1544-nm source was piezo modulated at 314 Hz with a sinusoidal modulation of amplitude 680 MHz, and the response was detected at the second harmonic. The resulting spectra recorded at 98 mbar for five concentrations are shown in Fig. 11, where we have plotted the normalised signal $u_{pp}$, i.e. the second-harmonic component divided by the DC component at the detector. Since the detector is AC coupled, the DC component cannot be measured directly. However, for a square wave with amplitude $V_{DC}$, the lock-in amplifier will measure the rms value of the fundamental Fourier component $2V_{DC}/\pi$, and we therefore take the DC value as $\pi/\sqrt{2}$ times the lock-in signal measured with the signal chopped at 314 Hz.

For quantitative analysis we follow the method outlined in [12], and again we choose to use line *a*. A crucial parameter is the modulation depth *b* defined as the ratio between the modulation amplitude 610 MHz and the HWHM line width. At 98 mbar and a broadening coefficient of 3.24 MHz/mbar the line width of 319 MHz is dominated by Lorentz broadening, and leads to $b = 1.912$. According to [12], $u_{pp}$ is related in the Lorentz limit to the line-centre absorbance $\gamma(0)$ as

$$u_{pp} = \gamma(0)\frac{F(b)}{\sqrt{2}}, \tag{7}$$

where $F(b)$ is an empirical function given by

$$F(b) = 1.02\frac{-0.52b^{0.12}+1}{0.55b^{0.12}+b^{-2}}, \tag{8}$$

which in the present case takes the value $F(1.912) = 0.515$. From this equation we can now determine the peak absorbance, and the concentration can be derived as in the preceding section. The results are given in Table 4 and again

| Nominal conc. (ppm) | second-harmonic analysis (ppm) |
|---|---|
| 4.1 | 4.2 |
| 8.3 | 8.0 |
| 13.5 | 14.3 |
| 20.7 | 19.7 |
| 30.6 | 30.2 |
| 49.3 | 47.0 |

**TABLE 4** Concentrations derived from second-harmonic analysis based on line *a* of lines *a–h*

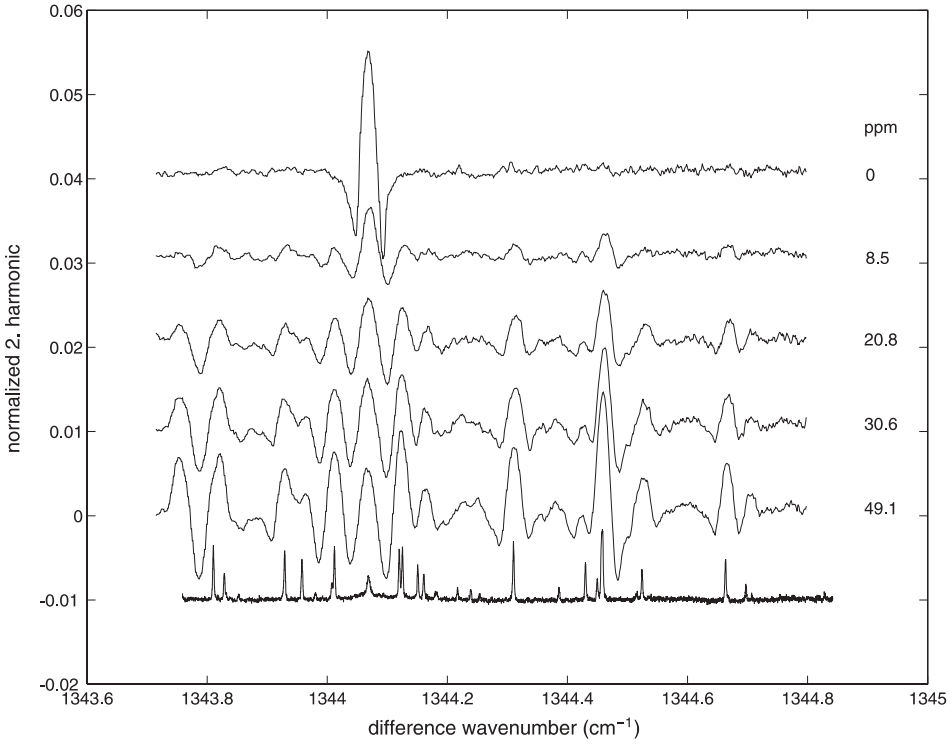


**FIGURE 11** Normalised second-harmonic spectra for a range of concentrations below 50 ppm. *Lower trace* is low-pressure reference spectrum of pure $SO_2$

we find perfect linearity, this time with a slope of $0.950 \pm 0.018$, and a zero intercept of $0.5 \pm 0.5$ ppm.

## 5 Uncertainty estimates

All uncertainties given in this section are standard uncertainties. The crucial parameter in the context of gas analysis is the line strength $S$ entering (4). When fitting the experimental absorption profile to a Voigt profile, the coefficient of $g(\nu - \nu_0)$ yields the combination $LSp/kT$, and $LS/kT$ is determined from a linear least-square fit of this coefficient versus the pressure $p$. The uncertainty of the slope is determined individually for each line, and reflects the experimental scatter. The uncertainty of the pressure calibration is taken as 2%, the cell length is $11.4 \pm 0.2$ mm, corresponding to 1.8%, and the temperature is taken as $298 \pm 2$ K, corresponding to 0.7%. The linearised frequency axis is checked by determining the line-centre positions of 20 lines covering a range of 22 GHz, using the line at $1344.31026\,\mathrm{cm}^{-1}$ as reference. The standard deviation of the difference between these values and those given in [11] is $0.00019\,\mathrm{cm}^{-1}$, corresponding to 6 MHz, which is identical to the experimental resolution, and the uncertainty associated with the frequency axis can therefore safely be neglected. The same applies to the uncertainty of the gas concentration, which is stated by the manufacturer to be 99.99%. The relative uncertainty components are added, and to the resulting uncertainty for the individual lines is further added a constant contribution of $0.08 \times 10^{-20}\,\mathrm{cm/mol}$, corresponding to 2% of the line strength of the strongest absorption feature. The latter contribution is an estimate of the error associated with baseline variations and with imperfect elimination of contributions from neighbouring lines. All uncertainty components are assumed to be uncorrelated, so that they can be added in quadrature. The resulting standard uncertainties as given in column 3 of Table 2 are about 4% for the strongest lines.

The Lorentz-broadening contribution emerging from the Voigt fit is proportional to pressure, and the broadening coefficient is determined from a linear least-square fit with individual uncertainties for each line, reflecting the experimental scatter of the points. As before, the uncertainty associated with pressure calibration is taken as 2%, and a contribution of 0.4 MHz/mbar is added to account for baseline variations and imperfect neighbour elimination. The resulting standard uncertainties are given in column 6 of Table 2. For nitrogen broadening the pressure range used was considerably higher than for self broadening, but this is to some extent compensated by the smaller broadening coefficient. Assuming the same uncertainty components as for self-broadening, we find the values given in column 7 of Table 2. Due to the smaller broadening coefficients, the relative uncertainties are larger than for self-broadening.

When deducing low-level gas concentrations from absorbance spectra, we face the same uncertainty contributions as when the line strengths were determined, and since different equipment is used, there is no correlation. The uncertainty of the base length of the White cell is taken as 0.5 mm, leading to a relative uncertainty of the absorption path length of 2.5%. The uncertainty of the pressure calibration is taken as 3%, and the uncertainty of the temperature as before is 0.67%. Combining with the 4% uncertainty of the line strength, cf. Table 2, we arrive at a total relative uncertainty of 5.6%. Adding finally a concentration-independent uncertainty component of 5 ppm to account for the baseline variations which eventually limit the sensitivity, we arrive at the values given in Table 3. Taking into account the 2% uncertainty quoted for the certified mixture, we find that our measured concentration for the undiluted mixture is consistent with the certificate. For the

diluted mixtures we also have to consider the uncertainty of the flow controllers. However, they were calibrated against a Brooks Volumeter to a relative accuracy of better than 0.5%, and hence do not add significantly to the uncertainty.

## 6 Discussion

We have demonstrated that a coherent source based on difference frequency generation in $AgGaSe_2$ can serve as a versatile and reliable tool for spectroscopy in the mid-infrared spectral range. The setup based on commercially available telecom equipment operated for extended periods with sufficient stability without the need for any active stabilisation of amplitude or frequency, and usually measurements could be initiated within 5 min after turning on the equipment. From the data given in [7] and [8] the conversion efficiencies for a 10-mm crystal length can be evaluated as $\eta = 9.3 \times 10^{-6}\,\mathrm{W}^{-1}$ and $\eta = 5.2 \times 10^{-5}\,\mathrm{W}^{-1}$ respectively, to be compared with our value of $\eta = 2.2 \times 10^{-5}\,\mathrm{W}^{-1}$. The lower value obtained by [7] can be explained by the fact that focusing was not optimised, and that not all of the generated power was intercepted by the $0.25 \times 0.25\text{-mm}^2$ detector. The difference between our result and that of [8] is not immediately understandable. However, it should be noted that their signal-to-noise ratio of 100 : 1 is somewhat lower that expected on the basis of the given detector characteristics, and that the output power could therefore have been overestimated.

A main purpose has been to assess the potential of the DFG source as a tool for performing quantitative analysis of gas mixtures at low concentrations. By using a line which is at the same time relatively strong and relatively well isolated from its neighbours, a $540 \pm 11$ ppm certified mixture was measured as $560 \pm 30$ ppm, and concentrations down to 4 ppm generated by dynamic mixing with pure $N_2$ were measured with deviations from the predicted concentrations generally not exceeding 10%. Although the largest uncertainty contribution comes from the line strength, the uncertainty budget appears to be rather well balanced, and a significant improvement of the overall uncertainty will require more accurate determination of the cell length and better control of the pressure, as well as elimination of residual background variations originating from optical imperfections in the system.

With the present cell we have a detection limit of about 1 ppm, and useful concentration measurements can be performed down to 4 ppm. It should be straightforward to push these limits by at least a factor of 10 by a corresponding increase of the absorption path length.

**ACKNOWLEDGEMENTS** This work has been supported by the Danish Science Research Council under Grant No. 9600860. Jes Henningsen wishes to acknowledge informative discussions with Frank K. Tittel during early phases of this work.

## REFERENCES

1 R. Kaarls, T.J. Quinn: Metrologia **34**, 1 (1997)
2 P. Werle: Spectrochim. Acta A **54**, 197 (1998)
3 J. Faist, F. Capasso, C. Sirtori, D.L. Sivco, J.N. Baillargeon, A.L. Hutchinson, S.N.G. Chu, A.Y. Chu: Appl. Phys. Lett. **68**, 3680 (1996)
4 F. Capasso, C. Gmachl: http://www.bell-labs.com/org/physicalsciences/psr/qc/
5 C.F. Dewey, L.O. Hocker: Appl. Phys. Lett. **18**, 58 (1971)
6 U. Simon, Z. Benko, M.W. Sigrist, R.F. Curl, F.K. Tittel: Appl. Opt. **32**, 6650 (1993)
7 K.P. Petrov, R.F. Curl, F.K. Tittel, L. Goldberg: Opt. Lett. **21**, 1451 (1996)
8 B. Sumpf, D. Rehle, T. Kelz, H.-D. Kronfeldt: Appl. Phys. B **67**, 369 (1998)
9 V.G. Dmitriev, G.G. Gurzadyan, D.N. Nikogosyan: *Handbook of Nonlinear Optical Crystals* (Springer, Berlin, Heidelberg 1991)
10 J. Henningsen, H. Simonsen: J. Mol. Spectrosc. **203**, 16 (2000)
11 L.S. Rothman, C.P. Rinsland, A. Goldman, S.T. Massie, D.P. Edwards, J.-M. Flaud, A. Perrin, C. Camy-Perot, V. Dana, J.-Y. Mandin, J. Schroeder, A. McCann, R.R. Gamache, R.B. Wattson, K. Yoshino, K.V. Chance, K.W. Jucks, L.R. Brown, V. Nemtchinov, P. Varanasi: J. Quantum Spectrosc. Radiat. Transfer **60**, 665 (1998)
12 J. Henningsen, H. Simonsen: Appl. Phys. B **70**, 627 (2000)